arXiv:1206.3834v1 [astro-ph.HE] 18 Jun 2012

The spectrum of high-energy cosmic rays measured with KASCADE-Grande

W.D. Apel [a], J.C. Arteaga-Velázquez [b,1], K. Bekk [a], M. Bertaina [d,1], J. Blümer [a,c], H. Bozdog [a], I.M. Brancus [e], P. Buchholz [f], E. Cantoni [d,g], A. Chiavassa [d], F. Cossavella [c,2], K. Daumiller [a], V. de Souza [h], F. Di Pierro [d], P. Doll [a], R. Engel [a], J. Engler [a], M. Finger [a], D. Fuhrmann [i], P.L. Ghia [g], H.J. Gils [a], R. Glasstetter [i], C. Grupen [f], A. Haungs [a,1], D. Heck [a], J.R. Hörandel [j], D. Huber [c], T. Huege [a], K.-H. Kampert [i], D. Kang [c,1], D. Kickelbick [f], H.O. Klages [a], K. Link [c], P. Łuczak [k], M. Ludwig [c], H.J. Mathes [a], H.J. Mayer [a], M. Melissas [c], J. Milke [a], B. Mitrica [e], C. Morello [g], G. Navarra [d,3], J. Oehlschläger [a], S. Ostapchenko [a,4], S. Over [f], N. Palmieri [c], M. Petcu [e], T. Pierog [a], H. Rebel [a], M. Roth [a], H. Schieler [a], F.G. Schröder [a], O. Sima [ℓ], G. Toma [e], G.C. Trinchero [g], H. Ulrich [a], A. Weindl [a], J. Wochele [a], M. Wommer [a], J. Zabierowski [k]

[a] *Karlsruher Institut für Technologie (KIT), Institut für Kernphysik, Germany*

[b] *Universidad Michoacana, Instituto de Física y Matemáticas, Morelia, Mexico*

[c] *Karlsruher Institut für Technologie (KIT), Institut für Experimentelle Kernphysik, Germany*

[d] *Dipartimento di Fisica dell' Università Torino, Italy*

[e] *National Institute of Physics and Nuclear Engineering, Bucharest, Romania*

[f] *Fachbereich Physik, Universität Siegen, Germany*

[g] *Osservatorio Astrofisico di Torino, INAF Torino, Italy*

[h] *Universidade São Paulo, Instituto de Física de São Carlos, Brasil*

[i] *Fachbereich Physik, Universität Wuppertal, Germany*

[j] *Department of Astrophysics, Radboud University Nijmegen, The Netherlands*

[k] *National Centre for Nuclear Research, Department of Cosmic Ray Physics, Łódź, Poland*

[ℓ] *Department of Physics, University of Bucharest, Bucharest, Romania*

Preprint submitted to Elsevier *19 June 2012*

Abstract

The energy spectrum of cosmic rays between 10^{16} eV and 10^{18} eV, derived from measurements of the shower size (total number of charged particles) and the total muon number of extensive air showers by the KASCADE-Grande experiment, is described. The resulting all-particle energy spectrum exhibits strong hints for a hardening of the spectrum at approximately $2 \cdot 10^{16}$ eV and a significant steepening at $\approx 8 \cdot 10^{16}$ eV. These observations challenge the view that the spectrum is a single power law between knee and ankle. Possible scenarios generating such features are discussed in terms of astrophysical processes that may explain the transition region from galactic to extragalactic origin of cosmic rays.

1 Introduction

The main goals of experimental cosmic ray research are the determination of the arrival direction distribution, the primary energy spectrum, and the elemental composition. Those measurements comprise important hints to understand the origin, acceleration and propagation of energetic cosmic particles. The needed measurements can be done directly or indirectly, depending on the energy of the primary particle. At energies above 10^{15} eV, the energy spectrum must be determined indirectly from the measured properties of extensive air showers (EAS) that cosmic rays induce in the Earth's atmosphere [1].

The determination of the primary energy and elemental composition in the energy range from 10^{15} eV up to above 10^{20} eV is subject of earth-bound experiments since more than five decades. It has been shown that the all-particle spectrum has a power-law like behavior ($\propto E^{-\gamma}$, with $\gamma \approx 2.7$) with features, which are known as 'knee' and 'ankle' at 3-5$\cdot 10^{15}$ eV and 4-10$\cdot 10^{18}$ eV, respectively. Whereas at the knee the spectrum steepens, the ankle is characterized by a flattening of the spectrum by roughly the same change of the spectral index of $\Delta\gamma = \pm 0.3$-0.4. Cosmic rays above the ankle are most probable of extragalactic origin [2], i.e. somewhere in the energy range from 10^{16} eV to a few 10^{18} eV a break-off of the heavy component and the transition of cosmic rays of galactic to extragalactic origin is expected.

As the measured position of the knee is roughly in agreement with the energy

[1] corresponding authors: Juan-Carlos Arteaga-Velázquez, Mario Bertaina, Donghwa Kang, *E-mail: haungs@kit.edu, spokesperson KASCADE-Grande*
[2] now at: Max-Planck-Institut für Physik, München, Germany
[3] deceased
[4] now at: University of Trondheim, Norway

where supernova remnants (SNR) become inefficient accelerating particles [3], various theories with different assumptions were developed to explain the behavior of the spectrum between the knee and ankle features.
The basic idea of the 'dip model' [4] is that the ankle is a propagation feature of extragalactic protons (energy loss by electron pair production). Consequently, in that model the composition at the ankle is to a large extent proton-dominant and the transition from galactic to extragalactic origin of cosmic rays occurs already at energies well below 10^{18} eV. In the scenario of the dip model, at energies around 10^{17} eV a pure galactic iron component should be left and a small kink in the spectrum at around 5-7$\cdot 10^{17}$ eV, as indicated by observations by the AKENO [5] and HiRes [6] experiments and named as 'second knee' [7], would be assigned to the transition. This is in agreement with the SNR theory, where the knee positions of individual primary masses are proportional to the charge of the nuclei starting with the proton knee at around $E^p_{knee} = 3$-$5 \cdot 10^{15}$ eV and $E^A_{knee} = Z \cdot E^p_{knee}$ (rigidity dependence of knee positions for galactic cosmic rays).
On the other hand, to avoid an early appearance of the extragalactic cosmic ray component, Hillas [3] proposed in addition to the standard SNR component, a 'component B' of cosmic rays of galactic origin. This component would also experience a charge dependence of break-offs, but now shifted to approximately ten times higher energy. As a result, the transition occurs here at the ankle and for the entire energy range from 10^{15} eV to 10^{18} eV a mixed elemental composition is expected. In this scenario, the second knee, if it exists, would be a feature of the component B.

The KASCADE experiment and its extension, KASCADE-Grande, aim to provide high quality air-shower data in the energy range of 10^{14} eV to 10^{18} eV to evaluate the validity of these models and to distinguish between them. The KASCADE experiment has shown that the knee is due to a distinct break in the proton intensity despite protons are not the most abundant primary in this energy range. The break is followed by a kink in the spectrum of Helium nuclei [8], i.e. the knee in the all-particle spectrum is a feature of the light nuclei (Z$<$ 6), only, where the difference in the energies of the knee features of primary protons and Helium facilitates the assumption of a charge dependence of the break-off. First analyses of KASCADE-Grande data [9] resulted in a knee-like feature at around $8 \cdot 10^{16}$ eV caused by a steepening in the spectrum of heavy primary cosmic rays. In the present analysis, the reconstruction of the all-particle energy spectrum of cosmic rays in the range from 10^{16} to 10^{18} eV is described in detail.

Depending on the experimental apparatus and the detection technique of ground-based air-shower experiments, different sets of EAS observables are available to estimate the energy of the primary cosmic ray [10]. In case of ground arrays the total number of charged particles (often called shower size) in the shower and the corresponding particle density at observation level are

commonly employed. The muon content of EAS plays an important role, too. In the atmosphere the muon component suffers less attenuation than electromagnetic or hadronic components and exhibits less fluctuations compared to the more abundant electromagnetic component. In KASCADE-Grande both components, the muon and the electromagnetic ones, are measured with independently operating detectors. Both, together with the information of their correlation on a single-event-basis, are used to derive the spectrum. After a short description of the apparatus and the reconstruction procedures of the EAS parameters, we will describe the method developed to determine the all-particle energy spectrum including studies of systematic uncertainties. We conclude this paper with a discussion of the results.

2 The Experiment

The experimental layout, as well as the reconstruction procedures and accuracies of KASCADE-Grande observables are described in detail in reference [11]. In this chapter, we only summarize the most important facts relevant for the present analysis.

2.1 KASCADE-Grande

The multi-detector experiment KASCADE [12] (located at 49.1°N, 8.4°E, 110 m a.s.l.) was extended to KASCADE-Grande in 2003 by installing a large array of 37 stations consisting of $10\,\mathrm{m}^2$ scintillation detectors each (Fig. 1). KASCADE-Grande provides a sensitive area of about $0.5\,\mathrm{km}^2$ and operates jointly with the existing KASCADE detectors. Main parts of the experiment used for the present analysis are the Grande array spread over an area of $700 \times 700\,\mathrm{m}^2$, and the original KASCADE array covering $200 \times 200\,\mathrm{m}^2$. The Grande array is installed over an irregular triangular grid with an average spacing of 137 m. The KASCADE array is composed of 252 detector stations on a square grid with 13 m spacing. It is organized in 12 outer clusters of 16 stations each and 4 inner clusters of 15 stations each. The outer clusters (192 stations) are equipped with two unshielded (e.m.) and one shielded (muon) detector units each. A muon detector unit consists of 4 plastic scintillators of $90 \times 90 \times 3\,\mathrm{cm}^3$ each, where the iron-lead shielding provides a threshold of 230 MeV kinetic energy for vertically incident muons. The total sensitive area of the muon array amounts to $622\,\mathrm{m}^2$.

While with the Grande array we reconstruct the total number of charged particles, data from the shielded scintillation detectors of the KASCADE array are used to reconstruct the total number of muons on an event-by-event basis for events triggered by Grande. The combination of both allows us to

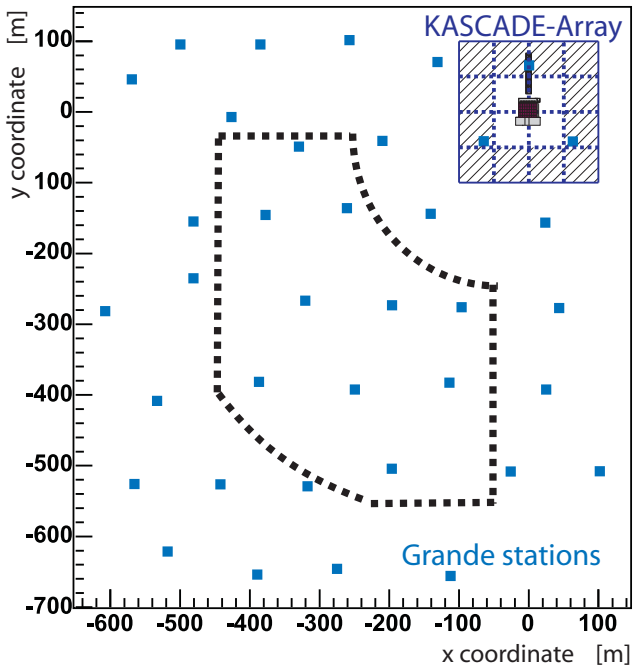

Fig. 1. Layout of the KASCADE-Grande experiment: The KASCADE array and the distribution of the 37 stations of the Grande array are shown. The outer 12 clusters of the KASCADE array consist of shielded μ-detectors (hatched area). The dotted line shows the fiducial area selected for the present analysis.

reconstruct the energy spectrum of cosmic rays in the range from 10^{16} eV up to 10^{18} eV.

2.2 Monte Carlo simulations

The simulations performed include the detailed air shower development in the atmosphere, as well as the response of the detector and its electronics. Therefore, the EAS parameters reconstructed from simulated showers are obtained exactly in the same way as for real data. The EAS were generated with uniformly distributed core positions (at an area larger than the Grande array), with isotropically distributed arrival directions, and with a spectral index of $\gamma = -2$, i.e. roughly one order of magnitude harder than the measured spectrum. The spectral slope is chosen as a compromise between computing time and statistical accuracy at the highest energies. Later, in the analysis procedures the simulated data is weighted to describe a softer energy spectrum with $\gamma = -3$. The EAS were simulated with CORSIKA [13] and the Monte Carlo generators FLUKA [14] and QGSJet II [15] (hadronic interactions). Sets of simulated events were produced in the energy range from 10^{15} eV to 10^{18} eV for five different representative mass groups: H, He, C, Si and Fe with about $353,000$ events per primary. A few showers for all primaries were also simulated for the higher energy range up to $3 \cdot 10^{18}$ eV in order to study the

reconstruction quality even beyond the energy range of interest. In addition, with less statistics, similar simulation sets were generated based on the high-energy hadronic interaction model EPOS, version 1.99 [16].

2.3 Reconstruction

Basic shower observables like the core position and the angle-of-incidence, as well as the total number of charged particles are provided by the reconstruction of data recorded by the Grande stations. The angle-of-incidence is determined using the relative particle arrival times at the stations. The core location, the slope of the lateral distribution function and the shower size (i.e. the total number of charged particles N_{ch}) are calculated by means of a maximum likelihood procedure, comparing the measured number of particles with the one expected from a NKG-like lateral distribution function [17] of charged particles in the EAS. KASCADE-Grande provides the unique opportunity of evaluating the reconstruction accuracies of the Grande array by a direct comparison with an independent experiment. For a subsample of events collected by the Grande array it is possible to compare on an event-by-event basis the two independent reconstructions of KASCADE and Grande. By means of such a comparison the Grande reconstruction accuracies of the total number of charged particles are found to be: systematic uncertainty $\leq 5\%$, statistical accuracy better than 15%; accuracy of the arrival direction of about 0.8°; accuracy of the core position about 6 m. The total number of muons N_μ is calculated using the core position determined by the Grande array and the muon densities ($E_\mu > 230\,\mathrm{MeV}$) measured by the KASCADE muon array detectors. N_μ is derived from a maximum likelihood estimation comparing the measured densities with a lateral distribution function, where the uncertainty is less than 12%. For the purpose of the present analysis, the estimated N_μ has been corrected for systematic uncertainties using a correction function, which is derived from Monte Carlo simulations as explained in appendix A.1. The correction improves the accuracy to better than 10%, including the uncertainty due to hadronic interaction models and unknown composition.

2.4 Data selection and shower size spectra

The selection used for the present analysis requires that the events passed successfully the full KASCADE-Grande reconstruction procedure. In addition, we requested events to be from stable periods of data taking with more than 35 Grande stations and all 16 KASCADE clusters in operation. The selected events had to pass a 7/7 Grande hardware trigger (six of a hexagonal shape and the central one) and had to hit more than 11 Grande stations in total.

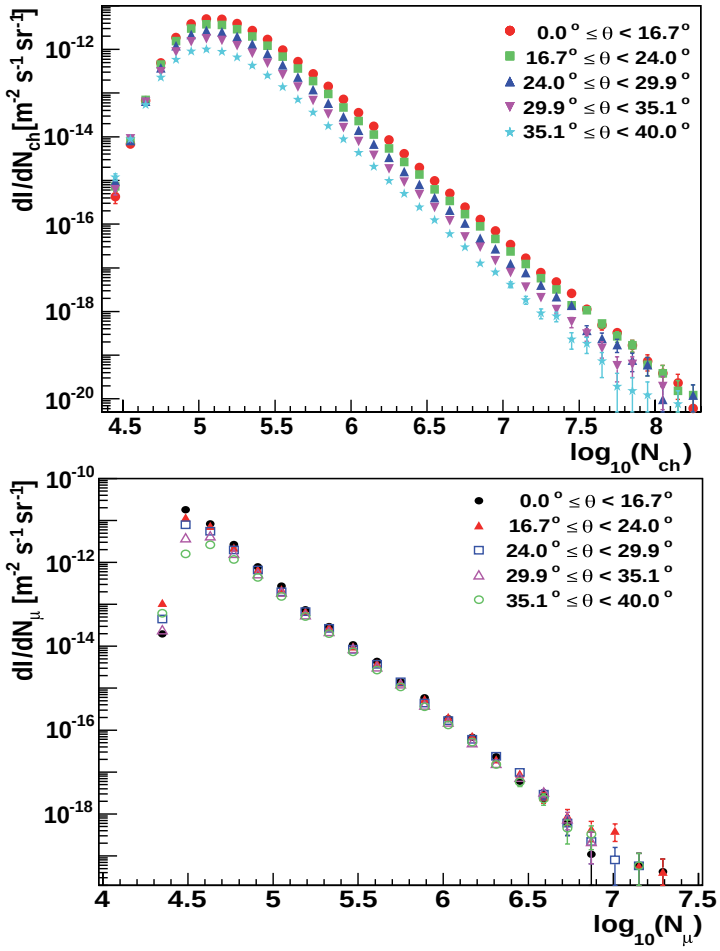

Fig. 2. Differential shower size N_{ch} and muon number N_μ spectra for different zenith angular ranges.

We restricted ourselves to events with zenith angles less than 40° due to increasing shower size uncertainties. Only air showers with cores located in a central area of KASCADE-Grande (see Fig. 1) were selected. With this cut on the fiducial area, border effects are discarded and the under- and over-estimations on the muon number for events close to and far away from the center of the KASCADE array are reduced. All of these cuts were applied also to the Monte Carlo simulated events to study their effects on the selection, to optimize the cuts, and to control the uncertainty of the acceptance. Full efficiency for triggering and reconstructing air-showers, as well as a uniform distribution of the shower cores in the fiducial area, is reached at a primary energy of about 10^{16} eV, slightly depending on the zenith angle, and on the primary particle type.

The analysis presented here is based on 1173 days of data. The cuts on the fiducial area and zenith angle result in a total acceptance of $1.98 \cdot 10^5\,\mathrm{m}^2{\cdot}\mathrm{sr}$, and an exposure of $2.0{\cdot}10^{13}\,\mathrm{m}^2{\cdot}\mathrm{s}{\cdot}\mathrm{sr}$, respectively. Approximately $1.5{\cdot}10^6$ events are subject of the following analysis.

Fig. 2 shows the reconstructed N_{ch} and N_{μ} distributions for five different angular ranges. The angular ranges were chosen in order to have the same acceptance in each of them.

3 The reconstruction of the all-particle energy spectrum

KASCADE-Grande, with the possibility of an independent reconstruction of the two observables N_{ch} and N_{μ} per individual EAS, allows us to go for a dedicated strategy in estimating the all-particle energy spectrum. By means of Monte Carlo simulations, calibration formulas are obtained to calculate the primary energy per individual event based on N_{ch} and N_{μ}, taking into account the correlation between the two particle components. This reduces the composition dependence of the energy assignment. To account for attenuation effects in the atmosphere, which are different for the two shower observables, the energy calibration is performed separately for the five zenith angular ranges. Finally, the obtained energy spectra are unfolded to account for the bin-to-bin migrations before they are combined to the resulting all-particle energy spectrum.

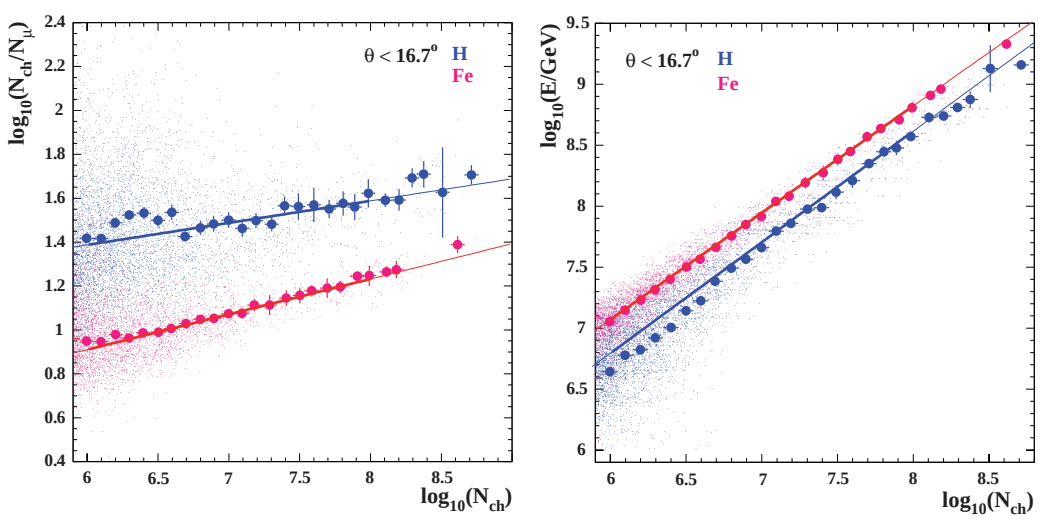

Fig. 3. Left panel: Scatter plot of the reconstructed N_{ch}/N_{μ} vs. N_{ch} for primary iron and proton nuclei and for the first angular bin. The full dots and error bars indicate the mean and statistical errors of the distribution of the individual events (small dots). The fits result in parameters c and d of expression 3. Right panel: Scatter plots of E vs. N_{ch} for iron and proton primary nuclei. The fits result in parameters a and b of expression 1.

3.1 Energy calibration

The energy assignment starts by applying $E = f(N_{ch}, k)$, where k is defined through the ratio of N_{ch} and N_μ: $k = g(N_{ch}, N_\mu)$. The main aim of the k parameter is to correlate these observables on an event-by-event basis, taking into account the differences in the N_{ch}/N_μ ratio for different primary masses with the same N_{ch}, as well as the shower-to-shower fluctuations for events of the same primary mass:

$$\begin{aligned} log_{10}(E/GeV) \;=\; & [a_H + (a_{Fe} - a_H) \cdot k] \cdot log_{10}(N_{ch}) + \\ & + b_H + (b_{Fe} - b_H) \cdot k \end{aligned} \tag{1}$$

$$k = \frac{log_{10}(N_{ch}/N_\mu) - log_{10}(N_{ch}/N_\mu)_H}{log_{10}(N_{ch}/N_\mu)_{Fe} - log_{10}(N_{ch}/N_\mu)_H} \tag{2}$$

$$log_{10}(N_{ch}/N_\mu)_{H,Fe} = c_{H,Fe} \cdot log_{10}(N_{ch}) + d_{H,Fe}. \tag{3}$$

By definition the k parameter is a number centered around zero for proton initiated showers and around one for iron initiated showers [18]. The coefficients a, b, c, d are obtained independently by simulations for each zenith angular range and for each primary mass, where fits are applied to the scatter plots $(N_{ch}, N_{ch}/N_\mu)$ and (N_{ch}, E). The fit range is chosen to be $6 \leq \log(N_{ch}) \leq 8$, i.e. where 100% trigger efficiency is guaranteed. Primary protons exhibit larger fluctuations than heavier primaries, therefore, the coefficients c and d are obtained iteratively in case of protons in order to improve the reconstruction of the energy spectrum. As an example, Fig. 3 shows the scatter plots including the resulting functions for the first angular bin. Shown are the errors on the mean, which are small due to the large Monte Carlo statistics. For the fits, however, we also take into account the width of the distributions in order to avoid a bias due to varying shower-to-shower fluctuations, in particular in case of primary protons and small shower sizes. It is obvious that taking into account the correlation of the observables reduces significantly the composition dependence of the energy assignment. Similar procedures are applied to the other angular bins and all the coefficients are compiled in Table 1. The uncertainties of these numbers are small, but considered in the calculation of the total systematic uncertainty.

Applying the derived energy calibration to the measured data, all-particle energy spectra for the five zenith angular ranges are obtained (Fig. 4). To refine the energy assignment function from the so far assumed pure power-law behavior of the $(N_{ch}, N_{ch}/N_\mu)$ and (N_{ch}, E) relations to a more realistic non-linear calibration, as well as to unfold bin-to-bin migrations due to shower-

Table 1
Coefficients of the energy calibration functions.

Angular bin	a		b		c		d	
	H	Fe	H	Fe	H	Fe	H	Fe
$\theta < 16.7°$	0.91	0.88	1.33	1.82	0.10	0.16	0.79	-0.06
$16.7° \leq \theta < 24.0°$	0.89	0.88	1.50	1.92	0.08	0.18	0.88	-0.25
$24.0° \leq \theta < 29.9°$	0.94	0.89	1.30	1.94	0.10	0.16	0.68	-0.17
$29.9° \leq \theta < 35.1°$	0.93	0.88	1.46	2.10	0.11	0.17	0.54	-0.35
$35.1° \leq \theta < 40.0°$	0.92	0.88	1.75	2.29	0.11	0.16	0.41	-0.35

to-shower fluctuations, response matrices R_{ij} for the different angular bins are constructed and applied, i.e. the spectra are unfolded (see appendix A.2). Effects of this procedure (see Fig. 4) on the flux are estimated to be smaller than 5% at all energy bins and, therefore, do not significantly change the shape of the spectra. For the following discussions we always refer to the unfolded spectra.

The spectra of the different angular ranges exhibit small systematic shifts relative to each other (see Fig. 4), where we observe a slight flux increase with increasing zenith angle. This corresponds to a horizontal shift in the energy assignment, which could be explained if real showers penetrate deeper in the atmosphere than predicted by the QGSJetII hadronic interaction model[5]. As the effect is observed for different assumed composition models and for all hadronic interaction models, it is most probably caused by a mismatch between the predicted and measured attenuation lengths of the shower particle numbers N_{ch} and N_{μ} (for a more detailed discussion see appendix A.3). The aforementioned differences in the spectra are considered as one of the major sources of the systematic uncertainty on the energy spectrum, and are taken into account in the estimation of the total systematic uncertainties. The final all-particle spectrum of KASCADE-Grande is obtained (see Figs. 6, 7, 8, and Table 3) by combining the spectra for the individual angular ranges. Only those events are taken into account, for which the reconstructed energy is above the energy threshold for the angular bin of interest (see Fig. 4).

3.2 Systematic uncertainties

Different sources of systematic uncertainties, which affect the all-particle energy spectrum, are investigated. Most of the effects lead to a shift in energy and this, in turn, to a shift in the spectrum (see also Table 2):

- Attenuation: The average difference between the intensities obtained for the

[5] In fact, the analysis of muon production heights with the muon tracking detector of KASCADE leads to a similar conclusion, see ref. [19].

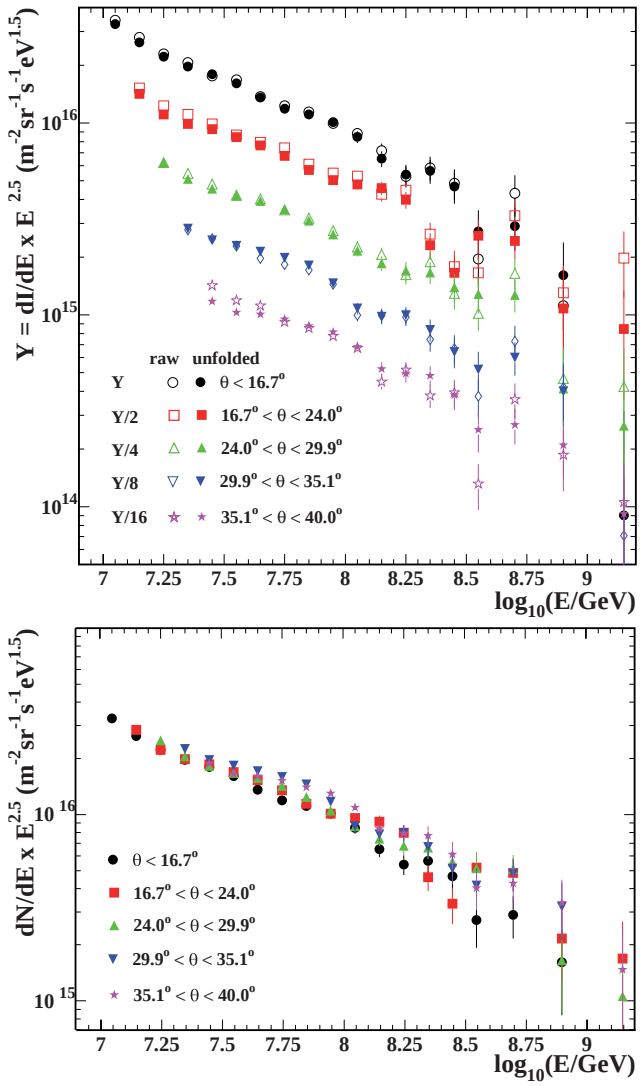

Fig. 4. Reconstructed all-particle energy spectra for all five angular bins. In the upper panel the direct reconstructed as well as the unfolded spectra are displayed, where the spectra are scaled for better visibility. In the lower panel only the unfolded spectra are shown without scaling. Only statistical uncertainties are displayed.

various angular bins has been used to define the systematic uncertainty associated with the angular dependence of the parameters appearing in the energy calibration functions of the different angular ranges. This includes the systematic uncertainty related to the description of the air shower attenuation in the atmosphere for simulated data. The uncertainty is used as well at lower energies, where not all angular bins contribute to the spectrum. In addition, this uncertainty indicates the limit for which the QGSjetII model reproduces the shower attenuation in a consistent way for the selected data sample.

- Energy calibration and composition: To estimate a possible bias in reproducing the energy spectrum, eqns. 1 and 2 have been applied to simulated energy spectra build up by pure H and Fe primaries as well as the other

Table 2
Estimated uncertainties of the cosmic ray intensity for different energies, where only absolute values are given in case of symmetric uncertainties.

Source of uncertainty	10^{16}eV (%)	10^{17}eV (%)	10^{18}eV (%)
intensity in different angular bins (attenuation)	−0/+6.5	10.9	21.3
energy calibration and composition	10.3	5.8	13.4
slope of the primary spectrum	4.0	2.0	1.9
reconstruction (core and shower sizes)	0.1	1.4	6.5
total	-11.1/+12.8	12.6	26.1
artificial spectrum structures (extreme cases)		<10	
hadronic interaction model (EPOS-QGSJet)	-5.3	-16.9	-14.6
statistical error	0.6	2.7	17.0
energy resolution (mixed composition)	24.7	18.6	13.6

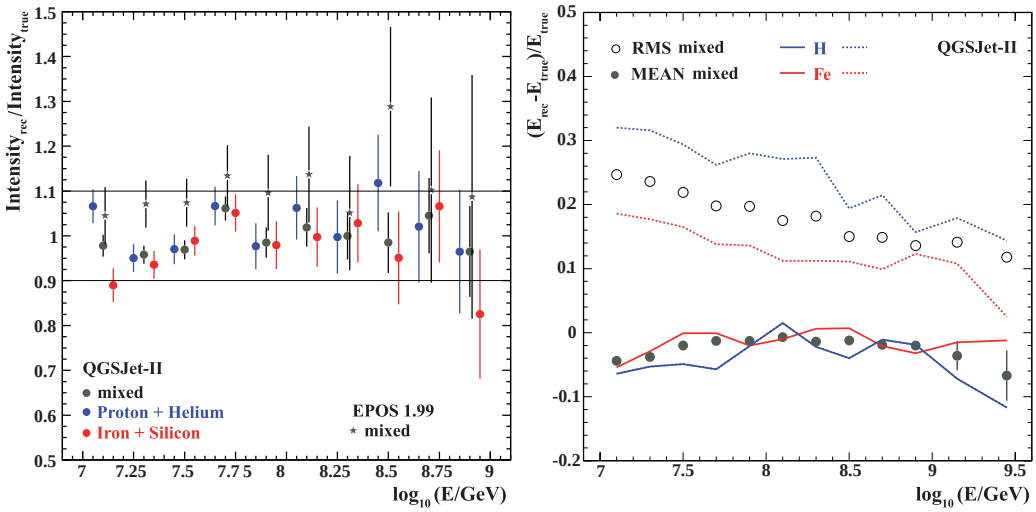

Fig. 5. Left panel: Ratio between the reconstructed and initially simulated energy spectrum for light (blue), heavy (red) and mixed primaries (black) summing up all angular bins. The ratio using simulated EPOS data when the spectrum is reconstructed using the QGSJet-II based calibration functions is also shown. The larger fluctuations are due to the lower statistics of the available EPOS simulations. Right panel: Resolution of the energy assignment for simulated sets (QGSJet) with mixed composition, pure proton, and pure iron primaries, respectively. The dots show the offsets of the reconstructed energy in bins of simulated energy for mixed composition, while lines represent the results for pure H and Fe assumptions. The circles and dotted lines show the corresponding RMS of these distributions.

three mass groups (He, C, Si), and by a uniform mixture of the five primaries with 20% abundance each. The spectra have been composed to fall off with slope γ = -3 and are compared with the reconstructed ones to find the corresponding uncertainty in intensity. Figure 5 summarizes the results on the ratio between the reconstructed and the initally simulated spectra for the full angular range. The original energy spectra are fairly well reproduced in all energy bins within a systematic uncertainty smaller than 10%. This

is quite important because it guarantees that any primary spectrum with arbitrary composition can be fairly well reproduced, even though the parameters of the response matrix and of the muon number correction functions have been defined on the basis of a mixed composition. Another important aspect to investigate is the capability and robustness of the analysis to recognize changes of the spectral shape and the elemental composition in the considered spectrum. Different cases have been simulated, from rigidity-dependent knees with variable abundances for each single chemical group to completely artificial compositions, such as sudden changes around 10^{17} eV from nearly pure iron to nearly pure protons and vice versa. Even for these extreme cases, the ratio between the reconstructed and initially simulated intensity deviates from unity throughout by less than 10%.

- Spectral slope of the Monte Carlo simulations: A further source of systematic uncertainty is the choice of a spectral slope of γ = -3 in the simulations to determine the energy calibration functions and response matrices. Therefore, new calibration functions and response matrices have been calculated using simulated spectra with γ_1 = -2.8 and γ_2 = -3.2. The difference between the intensities obtained with the new coefficients has been defined as systematic uncertainty and results into 4% at low energies, where the fluctuations are more important, and decreases to about 2% at E≈10^{17} eV.
- Reconstruction quality of shower sizes: The Grande array has an asymmetric geometry. Therefore, we checked the reconstruction of the observables by determining the energy spectrum for different ranges of distance of the shower core to the muon detector. The relative difference in intensity as a function of energy is used to compute a systematic uncertainty induced by the reconstruction, and it amounts to about 2% at around 10^{17} eV, slightly increasing with energy.
- Energy resolution: Simulated data using an equal mixture of all primaries have been divided in bins of true energy and the distributions of the relative differences between reconstructed and true energies have been compared. As shown in Fig. 5, right panel, the RMS of such distributions (energy resolution) is about 25% at lower energies and decreases to about 15% at the highest energies due to the decrease of intrinsic shower fluctuations. Results for pure H and Fe primaries are also indicated by lines. As expected, proton initiated showers show larger fluctuations compared to EAS generated by primary iron nuclei.
- Hadronic interaction models: By now, for all considerations the model combination QGSJet-II/FLUKA has been used. As the calibration depends on simulations, other interaction models may change the interpretation of the data. To study such effects we investigated the influence of the hadronic interaction model by performing the energy assignment based on simulations with the hadronic interaction model EPOS (version 1.99). Due to the smaller statistics of the EPOS simulations, larger uncertainties are obtained and no response matrix corrections could be applied. Therefore, a proper energy spectrum by means of EPOS simulations cannot be derived yet, but general

characteristics are inferred. Comparing the all-particle energy spectra for both cases, it was found that EPOS leads to a slightly lower intensity (≈10-15%) compared to QGSJet. A similar conclusion can be drawn, if the data simulated with EPOS are treated like experimental data and reconstructed using the QGSJet based calibration functions (see Fig. 5). Now, as a consequence, the intensity is reconstructed 10-15% higher than the simulated input. The main reason behind the difference between QGSJet and EPOS results has to be ascribed to the different N_{ch}/N_{μ} ratio predicted by the two models. In particular, EPOS predicts that the showers are richer in muons and slightly poorer in charged particles (for the relevant energy range, at sea level, and for the experimental conditions of KASCADE-Grande). These results are used as a rough estimate of the uncertainties due to the choice of the particular interaction model QGSJet-II.

3.3 Cross-checks of the energy spectrum reconstruction

Using the N_{ch}-N_{μ} ratio we reduced the dependence of the reconstructed all-particle spectrum on the elemental composition. But, since both observables are reconstructed independently, we can apply an energy spectrum reconstruction on both observables individually. At the end one would expect the same result for the energy spectrum by all approaches, provided that (i) the measurements are accurate enough, (ii) the reconstructions work without failures, and (iii) the Monte Carlo simulations describe correctly the shower development and its fluctuations, and (iv) the composition is known. But, the fact that not all of the above requirements are fulfilled and the individual observables exhibit substantial differences in their composition sensitivity hampers such straightforward cross-checks. Nevertheless, such analyses are used to check the reconstruction procedures and the influence of systematic uncertainties. Some details of these analyses [36,37] and the results can be found in appendix A.4.

In figure 6 the spectra obtained by the three methods are compiled, where the intensity is multiplied by a factor of $E^{3.0}$. Owing to the different approaches, the results using single observables are given only for the pure proton and iron assumptions, whereas the final spectrum is displayed with a band showing the systematic uncertainties. Using N_{ch} as the observable obtained from data of the Grande array only, a large dependence on the primary elemental composition is present, which is reflected in a big difference between the intensities for proton and iron assumptions. The muon number N_{μ} shows less composition dependence compared to the shower size, though it is still the largest contribution of uncertainty. The narrower range for a solution provided by N_{μ} compared to N_{ch} confirms the finding of KASCADE that at sea-level the number of mostly low-energy muons N_{μ} is less composition sensitive than the total number of charged particles [20]. The method finally applied for energy

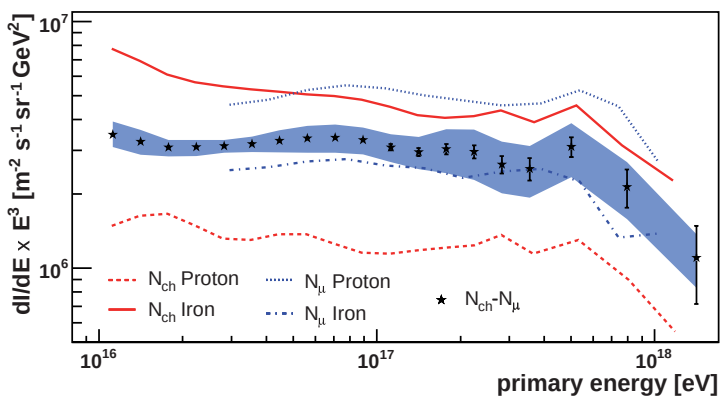

Fig. 6. Reconstructed all-particle energy spectrum by the three different approaches applied to KASCADE-Grande data. For the combined method a band is shown, indicating the range of the systematic uncertainty (without uncertainties due to the chosen hadronic interaction model).

estimation, owing to the combination of the two variables, results in a larger reconstruction uncertainty. But the total uncertainty (including composition dependence) is considerably smaller by taking into account also the correlation of these observables. This additional information is strikingly decreasing the composition dependence.

Of particular interest is the fact that by using N_{ch}, the iron assumption results in a higher intensity than the proton assumption, whereas using N_μ the opposite is the case (see appendix A.4). In any case, if there is only the possibility of applying a one-dimensional method, then one finds a large variance in possible solutions (any solution within the range spanned by the proton and iron line, not even parallel to these lines). Interestingly, over the whole energy range there is only little room for a solution satisfying both ranges, spanned by N_{ch} and N_μ, and this solution prefers a more heavy composition - in the framework of the QGSJet-II hadronic interaction model. The results obtained by combining N_{ch} and N_μ lie within the area spanned by the other methods. This finding expresses a cross-check of the intrinsic consistency of the results for the interpretation of two measured observables based on the used hadronic interaction model QGSJet-II. This was found to be valid also for the case of interpreting the data with the hadronic interaction model EPOS-1.99.

4 Results and discussion

The resulting all-particle spectrum exhibits structures which do not allow us to describe the spectrum with a single power law. To emphasize this, figure 7 shows the residuals of the all-particle energy spectrum multiplied by a factor in such a way that the middle part of the spectrum becomes flat. The power law index of $\gamma = -2.92 \pm 0.02$ is obtained by fitting the range of $\log_{10}(E/eV) =$

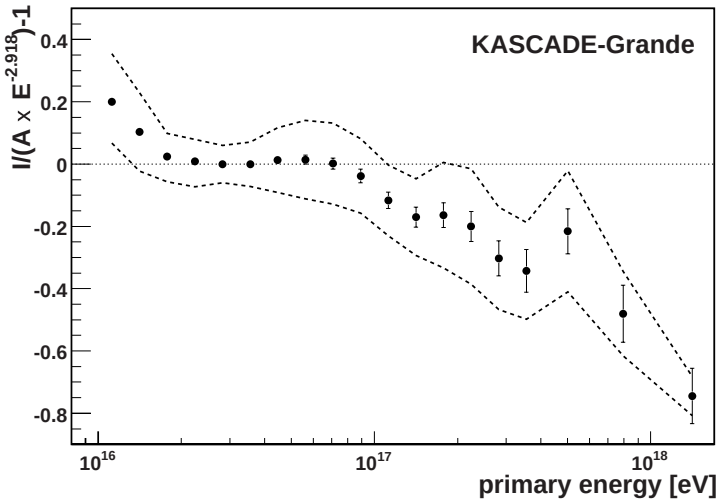

Fig. 7. The all-particle energy spectrum obtained with KASCADE-Grande. The residual intensity after multiplying the spectrum with a factor of $E^{2.918}$ and normalized with A is displayed as well as the band of systematic uncertainty.

Table 3
Differential intensity values of the all particle energy spectrum for the QGSJet-II based analysis. The first column of errors denotes the statistical uncertainty, the second column the systematic uncertainty.

bin number	Energy [eV]	$dI/dE \pm$ stat. $\pm$ syst. $[m^{-2}s^{-1}sr^{-1}GeV^{-1}]$
1	$1.11 \cdot 10^{16}$	$(2.46 \pm 0.02 \pm^{0.27}_{0.32}) \cdot 10^{-15}$
2	$1.41 \cdot 10^{16}$	$(1.16 \pm 0.01 \pm^{0.13}_{0.13}) \cdot 10^{-15}$
3	$1.78 \cdot 10^{16}$	$(5.49 \pm 0.03 \pm^{0.43}_{0.40}) \cdot 10^{-16}$
4	$2.24 \cdot 10^{16}$	$(2.76 \pm 0.02 \pm^{0.22}_{0.19}) \cdot 10^{-16}$
5	$2.82 \cdot 10^{16}$	$(1.40 \pm 0.01 \pm 0.08) \cdot 10^{-16}$
6	$3.55 \cdot 10^{16}$	$(7.13 \pm 0.07 \pm 0.50) \cdot 10^{-17}$
7	$4.47 \cdot 10^{16}$	$(3.69 \pm 0.04 \pm 0.38) \cdot 10^{-17}$
8	$5.62 \cdot 10^{16}$	$(1.89 \pm 0.03 \pm 0.23) \cdot 10^{-17}$
9	$7.08 \cdot 10^{16}$	$(9.52 \pm 0.17 \pm 1.24) \cdot 10^{-18}$
10	$8.91 \cdot 10^{16}$	$(4.67 \pm 0.11 \pm 0.58) \cdot 10^{-18}$
11	$1.12 \cdot 10^{17}$	$(2.19 \pm 0.07 \pm 0.28) \cdot 10^{-18}$
12	$1.41 \cdot 10^{17}$	$(1.05 \pm 0.04 \pm 0.16) \cdot 10^{-18}$
13	$1.78 \cdot 10^{17}$	$(5.41 \pm 0.26 \pm 1.10) \cdot 10^{-19}$
14	$2.24 \cdot 10^{17}$	$(2.64 \pm 0.16 \pm 0.61) \cdot 10^{-19}$
15	$2.82 \cdot 10^{17}$	$(1.12 \pm 0.10 \pm 0.28) \cdot 10^{-19}$
16	$3.55 \cdot 10^{17}$	$(5.66 \pm 0.59 \pm 1.34) \cdot 10^{-20}$
17	$5.01 \cdot 10^{17}$	$(2.47 \pm 0.23 \pm 0.61) \cdot 10^{-20}$
18	$7.94 \cdot 10^{17}$	$(4.26 \pm 0.75 \pm 1.11) \cdot 10^{-21}$
19	$1.41 \cdot 10^{18}$	$(3.90 \pm 1.36 \pm 0.96) \cdot 10^{-22}$

$16.2 - 17.0$. For the full energy range a statistical analysis reveals that the spectrum is not described by a single power law with a significance of 2.1σ.

Just above 10^{16} eV the spectrum exhibits a 'concave' behavior, which is significant with respect to the systematic and statistical uncertainties. This is true despite the fact that only vertical showers contribute to the spectrum in this energy range (see Fig. 4). This hardening of the spectrum is validated by several cross-checks, e.g., by efficiency correction of more inclined events based on simulations. A hardening of the spectrum is, on the one hand, expected when a pure rigidity dependence of the galactic cosmic rays is assumed. Depending on the relative abundances of the different primaries one would expect charge dependent steps (i.e. slope changes) in the all-particle spectrum. The gap in the knee positions of light primaries (proton, helium, and CNO group of $Z = 1 - 8$) and the heavy group can lead to a hardening of the spectrum [21]. On the other hand, there are also other possible astrophysical scenarios to get a concave behavior of the cosmic ray spectrum. In general, a transition from one source population to another one could also result in a hardening of the spectrum. In such a case, the KASCADE-Grande result could be a first experimental hint to the 'component B' of galactic cosmic rays, as proposed by Hillas [3]. A possible scenario for the component B is discussed by Ptuskin et al. [22], where the maximum acceleration energy for different types of supernovae is considered, taking into account also their relative abundances in our galaxy. This scenario can lead to an extension of the galactic component up to a few EeV. In addition, in this model the transition of CR origin from the standard type SN Ia to SN IIb supernovae requires a hardening of the spectrum at 10 PeV. General galactic modulation can lead only to a very smooth change of the slope index over more than a decade in energy, but postulating a contribution of a nearby (single) source, sharpening the knee at a few PeV [23,24], would also require a hardening of the spectrum just above 10 PeV. It is interesting to note that recently the CREAM detector (balloon experiment) has described such a hardening of the proton and helium spectra at much lower energies [25], which by the authors is assigned to a possible change of the acceleration mechanism of cosmic rays.

Another feature in the spectrum is a small break slightly below 10^{17} eV. Applying a second power law above 10^{17} eV an index of $\gamma = -3.39 \pm 0.07$ is obtained. The indices of the two power-laws differ from each other by two standard deviations. Even taking into account extreme scenarios for the systematic uncertainties, or applying more stringent procedures to calculate the significance an effect with $> 1\sigma$ remains. Fitting the spectrum with a function of two power laws intercepted by a smooth knee the energy of the break is assigned to $\log_{10}(E/eV) = 16.92 \pm 0.09$, which is in nice agreement to the value obtained by analysing the raw-like (i.e. not corrected for reconstruction uncertainties) all-particle spectrum [9]. In [9] it was also seen that the break gets more significant when analysing a subsample of events where showers generated by heavy primary particles are enhanced. The change in slope occurs at an energy where the charge dependent knee of the iron component would be expected (KASCADE QGSJet based analysis assigns the proton knee to

an energy of $\approx 3 \cdot 10^{15}$ eV). The change of the spectral index of this knee-like feature is small compared to the first one, original well-known knee [8], what could be explained, when the iron component is not dominant around 10^{17} eV. This again can happen in presence of a 'component B' of mixed composition, but a final conclusion is not possible without investigating the composition in detail.

Both observed features were subject to detailed cross-checks. In particular, we investigated how far the applied unfolding procedure affects the spectrum. To build up the response matrix an energy spectrum and a particular composition has to be assumed. We investigated possible effects by assuming extreme cases and by using different unfolding methods. If one assumes a very abrupt change of the spectral slope and in composition for a given energy, the resolution of KASCADE-Grande would indeed smear that out to a structure distributed over values of $0.3 - 0.5$ in $\log_{10}(\mathrm{E/eV})$ of the reconstructed spectrum, but still clearly visible.

At higher energies the KASCADE-Grande spectrum, in particular close to 10^{18} eV, where other experiments have claimed a 'second knee' [7], suffers from missing statistics.

Despite the fact, that the discussed spectrum is based on the specific hadronic interaction model QGSJet-II, there is confidence that the found structures of the energy spectrum remain stable. The analysis has shown that the applied procedure can reconstruct the total number of charged particles, as well as the total muon number sufficiently well, independently of the hadronic interaction model in use. But the energy calibration assumes that the QGSJet-II model provides the correct lateral distribution of the particles over the entire distance range (exceeding the geometrical size of KASCADE-Grande). First studies with an alternative method to reconstruct the energy spectrum via the particle density at a fixed distance give hints to systematic deviations [26] in the energy calibration of the observable. But, the spectral structures discussed above are also present in the results of these studies.

Figure 8 compiles the KASCADE-Grande energy spectrum with results of other experiments. Despite the independent measurements and data analysis there is a good agreement with the results of the KASCADE experiment and others in the overlapping energy range at low energies. In particular, the concave behavior seems to be needed to connect the spectrum with the spectra obtained by other experiments at the knee region. At higher energies the KASCADE-Grande spectrum (QGSJet-II) results in a slightly lower intensity compared to earlier experiments, in particular GAMMA, AKENO and YAKUTSK. The strong peak-like structure below 10^{17} eV as was claimed by the GAMMA experiment [27] is not confirmed by our results. At the highest energy accessible by the KASCADE-Grande experiment, where we suffer from

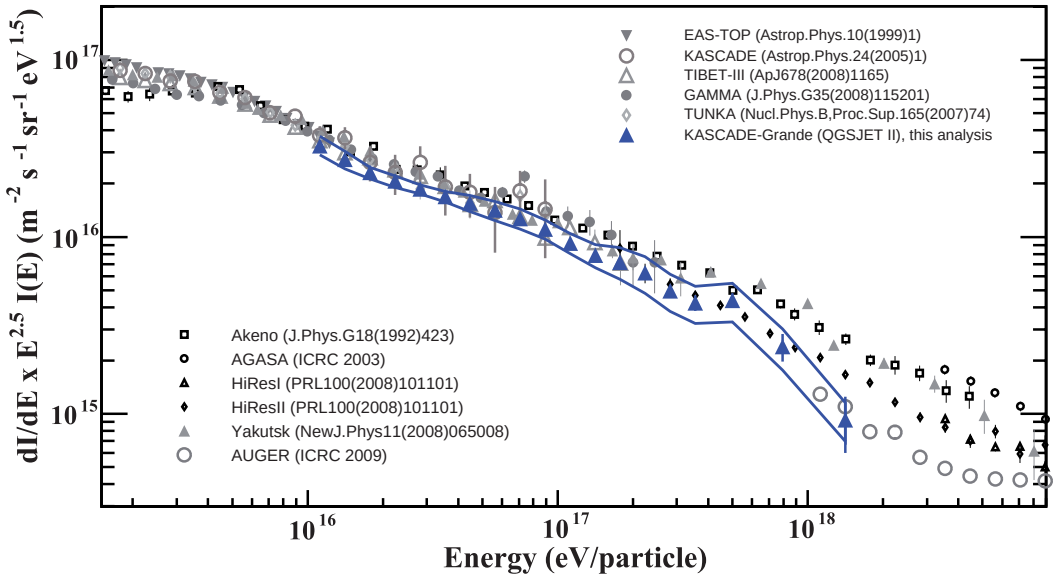

Fig. 8. Comparison of the all-particle energy spectrum obtained with KASCADE–Grande data based on the QGSJet-II model to results of other experiments. The band denotes the systematic uncertainties. An analysis based on EPOS 1.99 would result in a spectrum which is shifted downwards by approximately 10% in intensity.

missing statistics, our result is in agreement with a single power law and with the spectrum reported by HiRes and, when taken into account also the systematic uncertainties mentioned for the Auger result, with the Pierre Auger Observatory.

5 Conclusion

The main air-shower observables of KASCADE-Grande, shower size and total number of muons, are reconstructed with high precision and low systematic uncertainties. Applying various reconstruction methods to the KASCADE-Grande data the obtained all-particle energy spectra are compared as a way to cross-check the reconstruction, to study systematic uncertainties and to test the validity of the underlying hadronic interaction models. By combining both observables, the all-particle energy spectrum of cosmic rays is reconstructed in the energy range of 10^{16} eV to 10^{18} eV within an uncertainty in intensity of 10-15%, based on the hadronic interaction model QGSJet-II.

Correcting the spectra for reconstruction uncertainties and taking into account the systematic uncertainties for all methods, the underlying hadronic interaction models (QGSJet-II/FLUKA) result in a consistent solution, independent on the observable used, i.e. the single shower sizes or the correlation between the different observables. Tests with the hadronic interaction model EPOS 1.99 have shown that there is a shift in the absolute energy scale when

interpreting the data with this model, but the shape of the spectrum with its structures stays preserved. Progress in improving the interaction models is expected in the near future by detailed analyses of the now available data of the Large Hadron Collider, LHC (see, e.g. [28]).

The resulting spectrum is consistent, and in the overlapping energy range in a very good agreement, with results of the KASCADE, EAS-TOP, and other experiments (Fig. 8). The all-particle energy spectrum in the range from 10^{16} eV to 10^{18} eV is found to exhibit some smaller structures: In particular, a hardening of the spectrum is observed at $2 \cdot 10^{16}$ eV and a small break-off at around $8 \cdot 10^{16}$ eV. These features are used to discuss the astrophysics in the transition region from galactic to extragalactic origin of cosmic rays, where a final conclusion is not possible without detailed knowledge of the elemental composition in this energy range. However, amongst others, the model proposed by Hillas [3], e.g., which assumes a second component of galactic cosmic rays in addition to the standard SNR component, can explain the observed features of the measured all-particle energy spectrum.

A wealth of information on individual showers is available with KASCADE-Grande. This makes it possible to reconstruct the all-particle energy spectrum with high precision, as well as to investigate the elemental composition, to test hadronic interaction models, and to study cosmic ray anisotropies. All these studies are under way and further results are expected in the near future.

Acknowledgements

KASCADE-Grande is supported by the BMBF of Germany, the MIUR and INAF of Italy, the Polish Ministry of Science and Higher Education (this work partly by grant for 2009-2011). This work was partially supported by the Romanian Authority for Scientific Research CNCSIS-UEFISCSU grant PNII-IDEI no.461/2009, code 1442/2008 and project PN 09 37 01 05, and the German-Mexican bilateral collaboration grant (DAAD-Proalmex 2009-2012). J.C.A. acknowledges the partial support of CONACyT and the Coordinación de la Investigación Científica de la Universidad Michoacana.

A Appendix

A.1 Reconstruction of the total muon number

Due to the fact that the muon detectors are located at the fringe of the Grande array, the uncertainty of the reconstructed muon number grows is seen to increase with the distance of the KASCADE array to the shower core from about 5-10% at 250 m to 25% at 600 m for $\log_{10}(N_\mu) > 5.3$. But, as the features of these inaccuracies are well understood, we correct the reconstructed muon number by a correction function calculated on the basis of Monte Carlo simulations. This function takes simultaneously into account the dependence of the N_μ uncertainties on the zenith angle of the reconstructed air shower, on the distance of the core position from the KASCADE array in shower coordinates, and on the muon number. The correction function was found to be nearly independent from the composition of cosmic rays and from the hadronic interaction model used. The uncertainty after applying these corrections is less than 8% for total muon numbers above $\log_{10}(N_\mu) > 5.3$ (Fig. A.1), i.e. in the range of full efficiency.

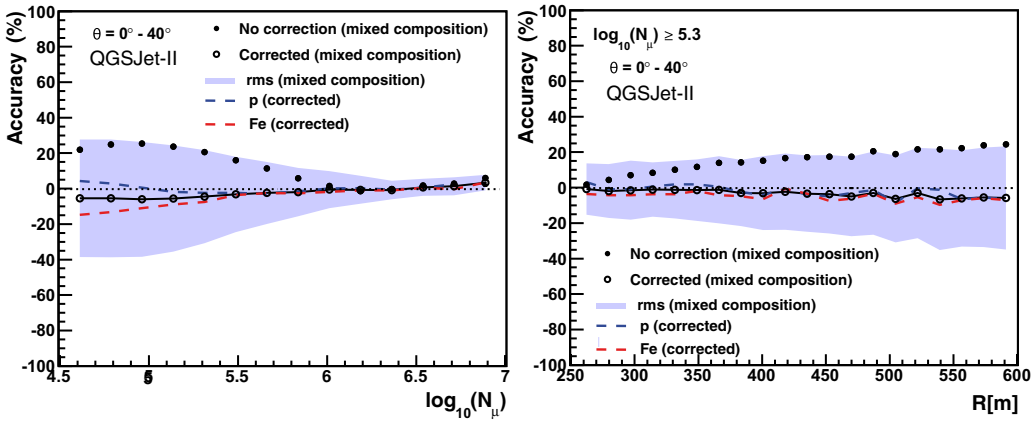

Fig. A.1. Accuracy ($\Delta N_\mu / N_\mu$ with $\Delta N_\mu = N_\mu^{True} - N_\mu$) of the reconstructed muon number before (solid circles) and after (open circles) applying the muon correction function versus the simulated muon size (left panel) and the distance of the EAS core to the KASCADE center (right panel). The lines represent the mean values of the achieved N_μ accuracy for different primaries after applying the correction function and the band, the corresponding one-sigma width for a mixed composition assumption.

As the fluctuations in the energy determination are larger than the bin size of the aimed-for energy spectrum an unfolding procedure is applied. Using Monte Carlo simulations a response matrix is constructed for the energy interval $\log_{10}(E/\mathrm{GeV}) = 6-9.5$, i.e. covering the entire range where fluctuations can affect the energy spectrum. This matrix represents the conditional probability, $P(E_j|E_i^{true})$, of an event with true energy in the bin $\log_{10}(E_i^{true})$ being reconstructed with energy $\log_{10}(E_j)$. By means of the response matrix a system of simultaneous equations, $n_j^{exp} = \sum_{i=1}^{N} P(E_j|E_i^{true}) n_i^{true}$, is established between the distribution of measured events, n_i^{exp}, and the actual energy distribution, n_i^{true}. The system is solved iteratively for the true distribution by means of the Gold-algorithm [29,30]. Statistical uncertainties on the data are taken into account during unfolding by multiplying the equation system by the error matrix $C_{ij} = \delta_{ij}/\sigma(n_j^{exp})$ [30]. The unfolding procedure involves also a van Cittert transformation of the equation system to guarantee the positive definiteness of the modified response matrix, which is a necessary requirement for the convergence of the method [29]. On the other hand, unfolded results are validated with another recursive method known as the Bayes-algorithm [31]. In general, both unfolding techniques perform in a stable way for the present application.

To avoid the problem of having wild fluctuations when increasing the number of iterations in the procedure a regularization method is applied, consisting of smoothing the result of unfolding in a given step before using it in the next iteration [31]. Smoothing was also applied to the response matrix, to avoid the presence of artificial effects in the unfolded distribution, which could arise from random fluctuations in some entries of the response matrix as a consequence of the limited statistics of the Monte Carlo data sets. Different methods for smoothing are applied and compared in order to find the optimal parameters for the procedure. To smooth the spectrum best results are obtained with the $353HQ$-twice algorithm [6] [32]. For the response matrix, quadratic fits along the diagonals are performed in the region of full efficiency to interpolate data into the region of low statistics. It is worth to mention that among the several tests employed to verify the performance of the methods, it was checked that the algorithms do not produce artificial structures in the spectrum or hide peaks which could be significantly present in the data, besides it was searched for the agreement between the forward-folded and measured distributions.

For a large number of iterations, both the Gold- and Bayes-algorithms converge to the same result in the energy interval of full efficiency and good statis-

[6] In each step of the iteration, k, the input spectrum, plotted as $\log_{10}[n_i^{(k-1)}]$ vs $\log_{10}(E_i^{true})$, is smoothed with the aforementioned algorithm.

tics. In addition, positiveness of the solution is observed. As one goes deeper in the number of steps, the weighted mean of the squared sum of statistical errors and systematic bias, i.e $(1/N)\sum_i^N(\sigma^2_{stat,i}+\sigma^2_{syst,i})/n_i^{true}$, decreases and becomes constant when the result converges. This parameter speaks about the quality of the final solution. Unfolding without smoothing was also tried, but, in general, poorer results were obtained.

A.3 Attenuation correction

In order to cross-check the attenuation effects of the observables N_{ch} and N_μ on the treatment in reconstructing the all-particle spectrum, we applied to the two estimated observable spectra a correction which is independent of Monte Carlo simulations. The Constant Intensity Cut Method (CIC method) is based on the assumption that the arrival direction distribution of cosmic rays is isotropic and that the cosmic ray intensity and composition changes monotonically with primary energy [33,34,35]. In this way, the intensity of primary particles becomes a reference variable for the primary energy of cosmic rays independent of the zenith angle. To apply the CIC method the integral spectra, $J(>N_{ch})$ and $J(>N_\mu)$, are calculated for all angular bins. Then, fixed frequency rates (integral intensities) are chosen in the range of maximum efficiency and sufficient statistics. By this, attenuation curves for each intensity are built, where an interpolation between two adjacent points of the integral spectrum is applied. The evolution of the shower size (muon number) in the atmosphere is extracted from the attenuation curves. The data have shown that it is possible to use constant attenuation parameters for the entire energy range since the differences in the obtained parameters by fitting individual curves are smaller than the uncertainty. With the parameters obtained, the shower size (muon number) of an individual air shower can be corrected with $N_{ch(\mu)}(\theta_{ref}) = N_{ch(\mu)}(\theta)\exp\left[P(\theta_{ref})-P(\theta)\right]$ to obtain the equivalent size at a given zenith angle of reference, θ_{ref}. The reference angle is chosen to be the mean of the measured zenith angle distribution, which is found to be 20° and 22° for the shower size and muon number distributions, respectively. Due to the independent reconstruction of N_{ch} and N_μ slightly different reconstruction thresholds lead to different mean angles and hence, different reference angles [36,37]. Uncertainties due to intrinsic assumptions on energy independent shower-to-shower fluctuations, the assumed spectral index, and constant composition are estimated and are taken into account. In Fig. A.2 the resulting spectra as corrected by the CIC method are shown for the shower size and for the muon number in the range of full efficiency for the independent reconstruction of the observables. Note that the bin sizes are selected according to the resolution of N_{ch} and N_μ. Applying this procedure to simulated data (QGSJet-II) has shown that indeed the differences between simulation and data are small for showers below 40° and that the estimated uncertainty on

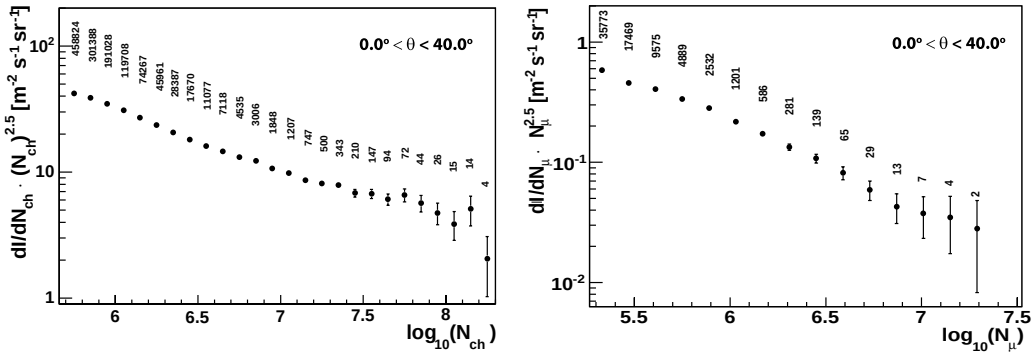

Fig. A.2. CIC corrected size spectra with statistical error bars and number of events per bin.

our all-particle spectrum is a conservative approximation.

A.4 Single parameter reconstruction of the energy spectrum

To reconstruct the energy spectrum by the observables independently, we use the reconstructed shower size spectra given in Fig. 2 and apply first an attenuation correction to the observables. Then, the shower size per individual event is calibrated by Monte Carlo simulations under the assumption of correlations in the form $E_0 \propto N_{ch}^{\alpha_{ch}}$ and $E_0 \propto N_\mu^{\alpha_\mu}$, respectively, and an assumed primary composition [36,37].

To determine the calibration function of the number of (attenuation corrected) charged particles N_{ch} and primary energy, Monte Carlo simulations were used, where a zenith angle range of $17° \leq \theta < 24°$, i.e. around the reference angle, was selected. Assuming a linear dependence in logarithmic scale: $\log_{10} E = a + b \cdot \log_{10} N_{ch}$, the correlation between the primary energy and the number of charged particles is obtained, where the fit is applied in the range of full trigger and reconstruction efficiencies (see left panel of Fig. A.3). The fit yields $a = 1.23$ and $b = 0.93$ for primary protons and $a = 1.75$ and $b = 0.90$ for iron primaries. The numbers confirm the assumption of a power law and show that the slopes of these power laws are very similar. However, the normalization parameters assigning the energy are very different for the two primaries. The fits are also performed for helium, carbon, silicon, and for a uniform mixed composition to examine the dependence of the calibration on the assumed primary particle type, where the values of the fit parameters are found to be in between the above values. The energy resolution is estimated from the difference between true and reconstructed energy, resulting in 32% and 18% at $E = 10^{17}$ eV for proton and iron primaries, respectively, with an energy dependence of approximately $1/\sqrt{E}$.

To determine the energy from the (attenuation corrected) total muon number

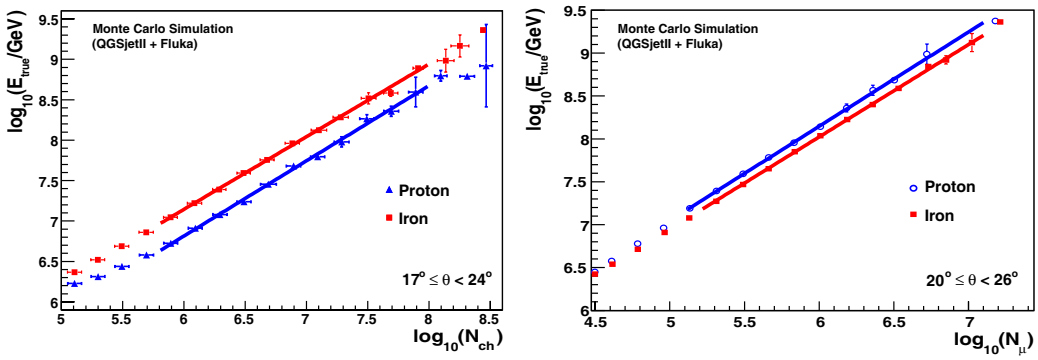

Fig. A.3. Calibration functions for assumed pure proton and iron primaries for the observables N_{ch} (left panel) and N_μ (right panel), respectively.

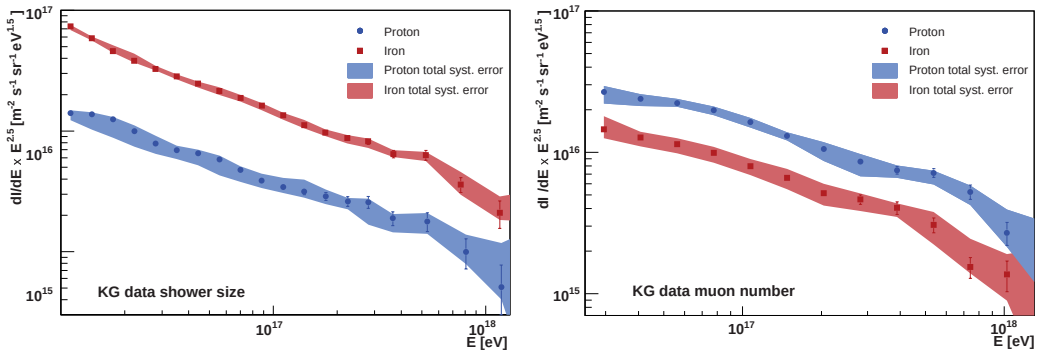

Fig. A.4. All-particle energy spectrum (including systematic uncertainties) for the assumption of primary protons and iron, respectively, based on the shower size (left panel) and on the total muon number (right panel).

N_μ a similar procedure as in the case of N_{ch} was applied: a calibration function for the muon size ($\theta_{ref} = 22°$) in terms of the primary energy was invoked. As before, the calibration curve is described with a relation of the form $\log_{10} E = a_\mu + b_\mu \cdot \log_{10} N_\mu$ (see Fig. A.3, right panel). For the case of pure protons, the fit results in $a_\mu = 1.61$ and $b_\mu = 1.09$ and for iron primaries the values $a_\mu = 1.63$ and $b_\mu = 1.07$ are obtained. Again it is observed that the slopes are similar, but here the difference in the parameter a is much smaller than in case of the charged particles. In case of the muon shower size, as the fluctuations are smaller, the energy resolution for protons and iron nuclei are of the order of 25% and 12% ($E \approx 10^{17}$ eV), respectively.

Figure A.4 shows the all-particle energy spectra as obtained after applying the calibration functions, as well as the corrections for the bin-to-bin fluctuations for both approaches. Apart from the statistical uncertainties also bands are shown describing the systematic uncertainties on the intensity, which were determined for the two approaches and different primaries independently. The considered sources of such uncertainties include the estimate of the calibration functions, the chosen reference angle for the calibration, the muon number correction function, and the application of the unfolding procedures. The total systematic uncertainty (i.e. sum in quadrature of all terms) on the intensity

for proton and iron is 21% (7%) and 10% (13%), respectively in case of N_{ch} (N_μ), at energies of 10^{17} eV. The systematic uncertainties are energy dependent and evolve in such a way that they slightly increase near the threshold, where fluctuations are larger, and in the high-energy region, where statistics decreases.

References

[1] M. Nagano and A.A. Watson., Rev. Mod. Phys. 72 (2000) 689.

[2] J. Abraham et al. (Pierre Auger Collaboration), Science **318** (2007) 939.

[3] A.M. Hillas, J. Phys. G: Nucl. Part. Phys. 31 (2005) R95.

[4] V. Berezinsky, A. Gazizov, S. Grigorieva, Phys. Rev **D74** (4) (2006) 043005.

[5] M. Nagano et al., J. Phys. G: Nucl. Part. Phys. **18** (1992) 423.

[6] R.U. Abbasi et al., PRL **100** (2008) 101101.

[7] D.R. Bergman and J.W. Belz, J. Phys. G: Nucl. Part. Phys. **34** (2007) R359.

[8] W.-D. Apel et al. (KASCADE Collaboration), Astrop. Phys. **24** (2005) 1.

[9] W.-D. Apel et al. (KASCADE-Grande Collaboration), Physical Review Letters **107** (2011) 171104.

[10] A. Haungs, H. Rebel, M. Roth, Rep. Prog. Phys. 66 (2003) 1145.

[11] W.-D. Apel et al. (KASCADE-Grande Collaboration), NIM A **620** (2010) 202.

[12] T. Antoni et al. (KASCADE Collaboration), NIM A **513** (2003) 429.

[13] D. Heck et al., Report FZKA 6019, Forschungszentrum Karlsruhe (1998).

[14] A. Fassò et al., Report CERN-2005-10, INFN/TC-05/11, SLAC-R-773 (2005).

[15] S.S. Ostapchenko, Nucl. Phys. B (Proc. Suppl.) **151** (2006) 143&147; S. Ostapchenko, Phys. Rev. D 74 (2006) 014026.

[16] K. Werner, F.M. Liu, T. Pierog, Phys. Rev. C **74** (2006) 044902.

[17] W.-D. Apel et al. (KASCADE Collaboration), Astrop. Phys. **24**, 467 (2006).

[18] M. Bertaina et al. - KASCADE-Grande Coll., NIM A (2012), doi:10.1016/j.nima.2012.01.008.

[19] W.-D. Apel et al. (KASCADE-Grande Collaboration), Astrop. Phys. **34**, 476 (2011).

[20] T. Antoni et al. (KASCADE Collaboration), Astrop. Phys. **6**, 245 (2002).

[21] C. De Donato, G.A. Medina-Tanco, Astrop. Phys. **32** (2009) 253.

[22] V. Ptuskin et al., Astrophysical Journal **718** (2010) 31.

[23] A.D. Erlykin and A.W. Wolfendale, J. Phys. G: Nucl. Part. Phys. **31** (2005) 1475.

[24] M. Shibata et al., Astrophysical Journal **716** (2010) 1076.

[25] H.S. Ahn et al., Astrophysical Journal **714** (2010) L89.

[26] G. Toma et al. - KASCADE-Grande Coll., Proc. 32th ICRC, Beijing (China), #icrc0405, vol.1/12, p.251.

[27] A.P. Garyaka et al., J. Phys. G: Nucl. Part. Phys. **35** (2008) 115201.

[28] D. d'Enterria et al., Astrop. Phys. **35** (2011) 98.

[29] R. Gold, Argonne National Laboratory Report ANL-6984, Argonne, 1964.

[30] H. Ulrich et al., KASCADE Collaboration, Proc. 27th ICRC, Hamburg, 2001.

[31] G.D. Agostini, DESY94-099 (1994); G.D. Agostini, NIM A **362** (1995) 487.

[32] J. Friedman, Cern School of computing, Norway, 22 (1974).

[33] D. M. Edge et al., J. Phys. **A6** (1973) 1612.

[34] M. M. Winn et al., J. Phys. **G12** (1986) 653.
M. Nagano et al., J. Phys. **G10** (1984) 1295.

[35] J. Alvarez-Muñiz et al., Phys. Rev **D66** (2002) 123004.

[36] D. Kang et al. - KASCADE-Grande Coll., Proc. 31th ICRC, Lodz (Poland) 2009, #icrc1044.

[37] J.C. Arteaga et al. - KASCADE-Grande Coll., Proc. 31th ICRC, Lodz (Poland) 2009, #icrc0805.